Euler Equations Analysis of the Initial Roll-Up of Aircraft Wakes

R. A. Mitcheltree*
North Carolina State University, Raleigh, North Carolina
R. J. Margason†
NASA Langley Research Center, Hampton, Virginia
and
H. A. Hassan‡
North Carolina State University, Raleigh, North Carolina

A new approach has been developed to study the initial roll-up of aircraft wakes. This approach is based on the solution of the three-dimensional Euler equations subject to inflow and initial conditions predicted by a vortex-lattice method. Thus, solutions are limited to those flowfields generated by wings that are free of flow separation. Results are presented for four configurations: a rectangular wing with part span flap, a rectangular wing, a typical transport-type configuration, and a fighter configuration. In addition, an assessment of an "unsteady two-dimensional analogy" was undertaken using the two-dimensional time-accurate Euler equation solutions in cross-flow planes. In general, predictions from the two-dimensional unsteady analogy coincided with the three-dimensional results, which were found to be in good agreement with available experimental data.

Introduction

IN terminal areas, the persistent trailing vortex system generated by large transport aircraft poses a serious threat to trailing aircraft. This restricts the flow of traffic in and out of large airports. The research presented here represents the results of the first phase of a research effort directed toward understanding the complex behavior of aircraft wakes. A final objective is the evaluation of methods for alleviation of the wake hazard. An excellent review of this problem is given by Donaldson and Bilanin.[1] According to Ref. 1, understanding aircraft wakes entails understanding four problems: the roll-up, interaction and stability, aging, and atmospheric effects.

The focus of this investigation is on the initial portion of the roll-up region. In this region, the length scale is on the order of the aspect ratio over the lift coefficient times the span length. As indicated in Refs. 1 and 2, processes in this region are essentially inviscid for wings that are free of flow separation. Thus, an approach based on the exact Euler equations should reproduce the experimentally observed features of this flowfield. Such an approach has a distinct advantage over other approaches reviewed in Refs. 1 and 2 because of the generality of the equations. This generality permits detailed study of the relevant flow dynamics and observation of the downstream evolution of the vortical structures in their proper spatial and temporal relationships.

In principle, the flowfield over the whole vehicle and in the wake can be calculated by solving the Euler equations in the entire region of interest. Unfortunately, present-day supercomputers do not have the combination of storage and processor speed required to facilitate adequate resolution of such a flowfield in a reasonable computational time. As a compromise, the three-dimensional Euler equations are used to study the wake region while a vortex-lattice method provides the inflow and initial conditions from an analysis of the lifting wing. The relationship between the wing and the computational domain is shown in Fig. 1. Present-day vortex-lattice methods are capable of calculating the flowfields past complex aircraft configurations at the low Mach numbers of interest here. Most of these methods assume the wake to be a flat sheet. Since the interaction of the wake with the generating configuration is weak, the cross-plane solution generated by the vortex-lattice at the trailing edge can be used to provide the inflow boundary condition for the Euler equations with only a small error.

Although only low Mach numbers are being considered, the compressible form of the Euler equations is employed. This is a crucial aspect of the formulation because the problem is dominated by free-flow boundaries (Fig. 1). It is not known a priori whether a side boundary is inflow or outflow. Therefore, to achieve an accurate solution, a procedure must be employed that selects the proper boundary condition at a given instant and point. The proper boundary conditions for the compressible Euler equations, which are hyperbolic, are determined by the method of characteristics.[4] These have been implemented here.

The Euler equations are solved using a fourth-order Runge-Kutta time-stepping method similar to the widely used method of Jameson et al.[5] With this method, the use of numerical damping is required. It is extremely important that the effects of numerical damping be reduced to a minimum so that the relevant physics of the problem is not masked. Only fourth-difference damping has been used. It should have little influence on the accuracy of the present second-order scheme.

Use of the compressible Euler equations to describe a low Mach number flow results in a system of stiff equations that renders the Runge-Kutta time-stepping scheme inefficient. The stiffness is a result of the fact that the speed of sound a is much higher than the flow velocity u. Physical properties in the flowfield are changing over time scales on the order of $1/u$, whereas the time scale for the Runge-Kutta scheme is restricted to the much smaller quantity of $1/(u+a)$. An ac-

Received Dec. 6, 1985; presented as Paper 86-0078 at the AIAA 24th Aerospace Sciences Meeting, Reno, NV, Jan 6-9, 1986; revision received April 1, 1986.

*Research Assistant, Mechanical and Aerospace Engineering. Student Member AIAA.

†Head, Analytical Methods Branch, Low-Speed Aerodynamics Division. Associate Fellow AIAA.

‡Professor, Mechanical and Aerospace Engineering. Associate Fellow AIAA.

celeration scheme proposed by Turkel[6] to overcome this stiffness has been assessed in the present paper.

Previous solutions[7,8] based on the Navier-Stokes/Euler equations made use of an "unsteady two-dimensional analogy." This analogy replaces the three-dimensional equations with the two-dimensional unsteady equations. Each stage in the time evolution of the unsteady equations is then associated with an equivalent downstream location by assuming uniform streamwise velocity. Such an assumption ignores the streamwise velocity variations. The code developed here is used to examine the accuracy of the unsteady analogy. This represents the first attempt at using a single code to compare the results of a two-dimensional unsteady wake calculation with the three-dimensional steady-state calculation.

Computations for the configurations examined were utilized in different ways. The flapped-wing configuration was used primarily to assess the validity of the unsteady analog and determine the benefit of Turkel's covergence acceleration scheme. The rectangular-wing calculations were compared with the measurements of Chigier and Corsiglia[9] and the calculations of Ref. 8. The transport configuration calculations were also compared with those of Ref. 8. Finally, the capabilities of the method are further demonstrated by considering a fighter configuration.[10]

Analysis

As previously indicated, the method selected to examine this complex flowfield involves a split-solution technique. The vortex-lattice method used to generate the wing solution is discussed in Ref. 10. The remainder of this analysis section will describe the formulation and method of solution of the Euler equations in the wake region.

Governing Equations

The conservation law form of the Euler equations in time-independent curvilinear coordinates, i.e.,

$$\xi=\xi(x,y,z), \qquad \eta=\eta(x,y,z), \qquad \zeta=\zeta(x,y,z) \tag{1}$$

can be written as

$$\frac{\partial q}{\partial t}+\frac{\partial F}{\partial \xi}+\frac{\partial G}{\partial \eta}+\frac{\partial H}{\partial \zeta}=0 \tag{2}$$

where

$$q=J(\rho,\rho u,\rho v,\rho w,\rho E)^T \tag{3}$$

$$F=J(\rho U,\rho uU+\xi_x p,\rho vU+\xi_y p,\rho wU+\xi_z p,\rho Uh)^T \tag{4}$$

$$G=J(\rho V,\rho uV+\eta_x p,\rho vV+\eta_y p,\rho wV+\eta_z p,\rho Vh)^T \tag{5}$$

$$H=J(\rho W,\rho uW+\zeta_x p,\rho vW+\zeta_y p,\rho wW+\zeta_z p,\rho Wh)^T \tag{6}$$

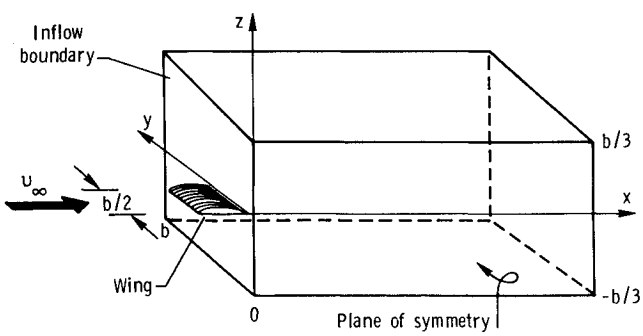

Fig. 1 Physical relationship between the wing and the Euler computational domain.

$$J=x_\xi(y_\eta z_\zeta-z_\eta y_\zeta)+y_\xi(z_\eta x_\zeta-x_\eta z_\zeta)+z_\xi(x_\eta y_\zeta-y_\eta x_\zeta) \tag{7}$$

$$U=\xi_x u+\xi_y v+\xi_z w \tag{8}$$

$$V=\eta_x u+\eta_y v+\eta_z w \tag{9}$$

$$W=\zeta_x u+\zeta_y v+\zeta_z w \tag{10}$$

u, v, and w are the velocity components in the x, y, and z directions, respectively, ρ is the density, p the pressure, E the stagnation internal energy, and h the stagnation enthalpy. Grid stretching is employed so that

$$\xi=\xi(x) \qquad \eta=\eta(y) \qquad \zeta=\zeta(z) \tag{11}$$

A finite-difference method is used to solve the governing equations. Central-difference operators are used in all directions. In order to suppress odd-even point decoupling in the numerical solution, an explicit fourth-difference smoothing term is added. Equation (2) can then be written as

$$\frac{dq}{dt}+Lq-Dq\equiv\frac{dq}{dt}+R(q)=0 \tag{12}$$

L is the central-difference operator and Dq is the smoothing term,

$$Dq=J\beta[(\nabla_\xi\Delta_\xi)^2+(\nabla_\eta\Delta_\eta)^2+(\nabla_\zeta\Delta_\zeta)^2](q/J) \tag{13}$$

where β is a parameter. A fourth-order Runge-Kutta time-stepping scheme is employed to advance the solution of Eq. (2) in time toward a steady-state solution. The scheme can be written as:[11]

$$q^{n+1}=q^m \qquad m=4$$

with

$$q^0=q^n \tag{14}$$

$$q^j=q^n-\alpha_j\Delta tR(q^{j-1}), \qquad j=1,2,\ldots,m$$

$$\alpha_1,\alpha_2,\alpha_3,\alpha_4=1/4 \;\; 1/3 \;\; 1/2 \;\; 1$$

Boundary Conditions

Equation (2) can be written in the form

$$\frac{\partial q}{\partial t}+A\frac{\partial q}{\partial \xi}+B\frac{\partial q}{\partial \eta}+C\frac{\partial q}{\partial \zeta}=0 \tag{15}$$

where A, B, and C are 5×5 matrices defined as

$$A=\frac{\partial F}{\partial q} \qquad B=\frac{\partial G}{\partial q} \qquad C=\frac{\partial H}{\partial q} \tag{16}$$

The five simultaneous equations given by Eq. (15) are hyperbolic. Hence, each of the matrices A, B, and C have five real eigenvalues that are the characteristic velocities in each of the spatial directions. For subsonic flow oriented in the direction of increasing coordinates, four of the eigenvalues are positive and one is negative. Thus, at an inflow boundary, four boundary conditions need to be specified while the fifth is extrapolated from within the computational domain. On the other hand, at an outflow boundary, one condition needs to be specified while the other four are extrapolated.

Detailed derivation of the boundary conditions, which are referred to as characteristic variable boundary conditions, are given in Ref. 4. As an illustration, consider the boundary conditions of boundaries normal to the ξ direction. Using a similarity transformation, the matrix A can be wirtten as

$$A=P\Lambda P^{-1} \tag{17}$$

where P is a matrix whose columns are the eigenvectors of A. P^{-1} is the inverse of P, and Λ is a diagonal matrix whose elements are the eigenvalues of A, i.e.,

$$\lambda_1,\lambda_2,\lambda_3 = \xi_x u + \xi_y v + \xi_z w$$
$$\lambda_4 = \lambda_1 + a \mid \nabla\xi \mid$$
$$\lambda_5 = \lambda_1 - a \mid \nabla\xi \mid \tag{18}$$

Where a is the speed of sound. The characteristic varibles Q are given by

$$Q = P^{-1}q \tag{19}$$

Thus, at a subsonic inflow boundary where $\lambda_1,\lambda_2,\lambda_3,\lambda_4 > 0$, the boundary conditions are

$$Q_{k,b} = Q_{k,\infty}, \qquad k = 1,\ldots,4; \qquad Q_{5,b} = Q_{5,e} \tag{20}$$

where subscriptions e, b, and ∞ refer to the interior, boundary, and infinity points, respectively. Similarily, for a subsonic outflow,

$$Q_{k,b} = Q_{k,e}, \qquad k = 1,\ldots,4, \qquad Q_{5,b} = Q_{5,\infty} \tag{21}$$

Similar relations hold at boundaries normal to the η and ζ directions.

In this approach, the velocities determined by the vortex-lattice method and the known stagnation enthalpy provide the four conditions required at the inflow boundary. At the outflow boundary, the pressure was specified to be that of the freestream.

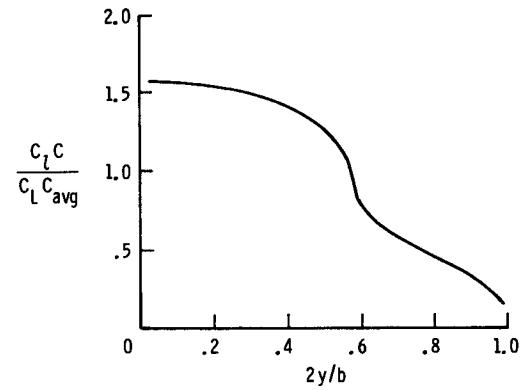

Fig. 2 Spanload distribution for the rectangular wing with part-span flap configuration.

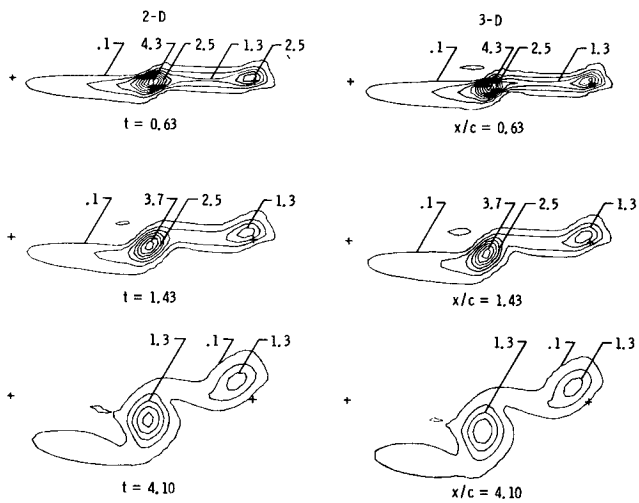

Fig. 3 Rectangular wing with flap, comparison of two- and three-dimensional vorticity contour plots.

Convergence Acceleration Scheme

When using an explicit time-stepping scheme, the time step is controlled by the maximum eigenvalue which, in this case, is λ_4. The physical properties change over time scales that are inversely proportional to the flow velocity. Turkel[6] showed that the use of a preconditioning matrix makes it possible to advance the solution using a time step independent of the speed of sound. This is achieved by modifying Eq. (2) to the form

$$M^{-1}q_t + \frac{\partial F}{\partial\xi} + \frac{\partial G}{\partial\eta} + \frac{\partial H}{\partial\zeta} = 0 \tag{22}$$

where

$$M^{-1} = I + \mathrm{d}N, \qquad M = I + eN \tag{23}$$

$$N = \begin{vmatrix} s^2 & -u & -v & -w & 1 \\ us^2 & -u^2 & -uv & -uw & u \\ vs^2 & -uv & -v^2 & -vw & v \\ ws^2 & -wu & -wv & -w^2 & w \\ hs^2 & -uh & -vh & -wh & h \end{vmatrix} \tag{24}$$

$$s^2 = \frac{(u^2+v^2+w^2)}{2}, \quad d = \frac{(\gamma-1)}{a^2}\left(\frac{a^2}{z^2}-1\right)$$
$$e = \frac{(\gamma-1)}{a^2}\left(\frac{z^2}{a^2}-1\right)$$
$$z^2 = \max(\epsilon, s^2), \quad \epsilon \sim 0.01u \tag{25}$$

Results and Discussion

The approach presented here can be used in conjunction with any production panel method code. In this work, the vortex-lattice method (VLM) of Margason and Lamar[10] is employed. This VLM has been shown[3] to be as accurate as any of the more complicated panel methods for predicting overall aerodynamic coefficients and spanload distributions. The VLM calculations provide the velocities at the inflow boundary (i.e., $x = 0$ in Fig. 1) and the initial conditions for the Euler equations.

As an illustration of this approach, four geometries are considered. The first geometry[12] is that of an aspect ratio 5.9 rectangular planform wing with a part span flap deflected 30 deg. The VLM requires specification of C_L, then α is calculated as

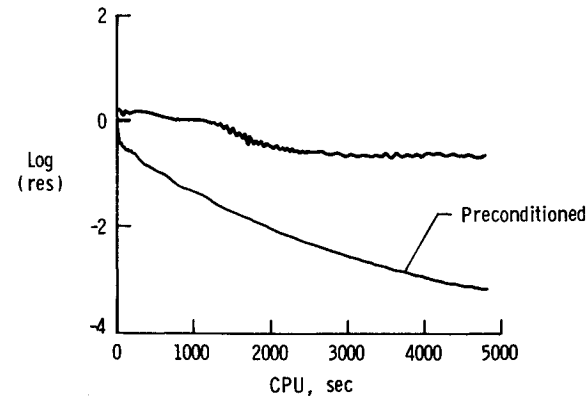

Fig. 4 Effect of matrix preconditioning on convergence rate.

part of the solution. The lift coefficient for this arrangement is 1.1 and the corresponding α is 4 deg. This geometry is used primarily to conduct a number of numerical experiments. These experiments assess the accuracy of the unsteady analogy and the usefulness of the convergence acceleration scheme. This geometry is selected for the numerical experiments because VLM predicts that it involves the greatest axial velocity gradients of the cases examined in this paper. For this geometry, u_{max} at the initial plane is on the order of $(1.2\ u_\infty)$, while for the other geometries, it is on the order of $(1.05\ u_\infty)$. Thus, this geometry should present the most difficult "test" of the two-dimensional analogy.

The spanload distribution for this first configuration is shown in Fig. 2. The distribution's shape reflects the presence of the flap. Figure 3 compares the predictions of the three-dimensional steady-state calculations with those determined from the two-dimensional unsteady calculations. The results display the lines of constant streamwise vorticity for the half-plane. The plus (+) signs in the figure show the equivalent locations of the wing root and tip. It should be indicated that the three-dimensional calculation used 31 stations in the axial direction corresponding to x/c from 0.0 to 4.1. As seen in Fig. 3, the vorticity contours from both calculations are in good agreement at all stations. This agreement suggests that the unsteady analogy is a good approximation even in the presence of axial velocity gradients of the magnitude considered in this case. It should also be noted that the three-dimensional calculation required two orders of magnitude more computer time than the corresponding two-dimensional calculation.

The effect of Turkel's matrix preconditioning[6] on the convergence rate is shown in Fig. 4. In this calculation the initial solution for the three-dimensional calculation was obtained from the unsteady two-dimensional analogy. As is seen in the figure, Turkel's preconditioning is beneficial.

The effects of varying the smoothing coefficient β [see Eq. (13)] and refining the computational grid were examined. Values of β ranging from 0.2 to 0.8 were employed. The value of β was found to have an effect on the magnitude of the resulting peak vorticity. However, it did not affect the position of the core or the state of vorticity roll-up. The number of grid points was doubled in each of the spanwise and streamwise directions, with insignificant effect on the peak vorticity decay. Thus, the results presented here are independent of the grid sizes evaluated herein (61×31 and 121×31). However, due to limits in computer storage, these grids are still rather coarse relative to core dimensions.

The second geometry examined was a rectangular planform wing of aspect ratio equal to 5.9. The span-load distribution for a lift coefficient of 0.5 ($\alpha=4$ deg) is presented in Fig. 5. Comparisons are made first with the experiment of Chigier and Corsiglia,[9] which was carried out in the Ames 7×10 ft wind tunnel. Since the flow in the tunnel is turbulent, the vortex wake position tends to be unsteady in the roll-up region. This meandering, as it is called, makes accurate measurement of velocity profiles difficult. Figure 6 compares the measured axial and tangential profiles (for $\alpha=8$ deg) through the core to the numerically computed values. It is seen that despite the scatter in the experimental data, good agreement is indicated. Figure 7 plots the streamwise variation of u_{max} and core location. Both the experimental measurements and the numerical predictions were for $\alpha=12$ deg. Again, good agreement is indicated.

Comparisons with other numerical calculations are discussed next. As indicated in Ref. 1, the length of the roll-up

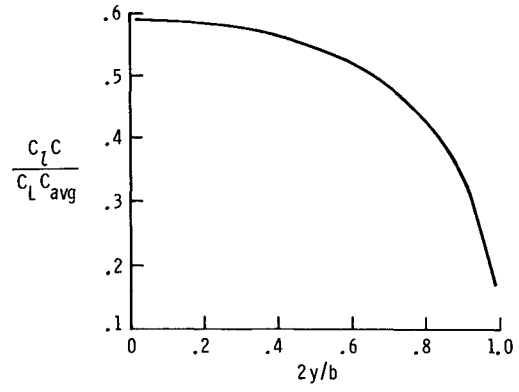

Fig. 5 Spanload distribution for the rectangular wing configuration.

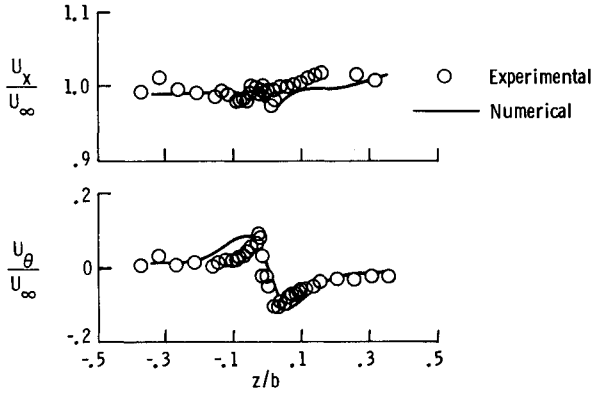

Fig. 6 Rectangular wing, core axial and tangential velocity distributions.

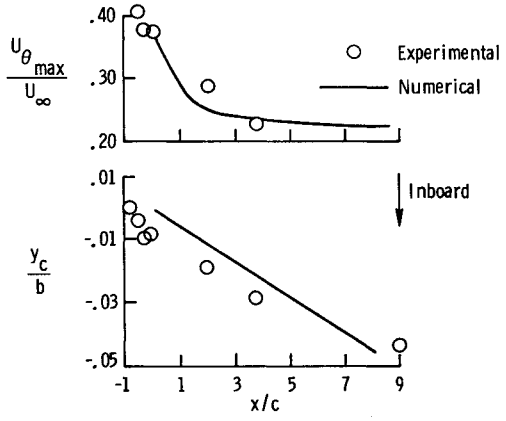

Fig. 7 Rectangular wing, effect of variation of axial distance on $u_{\theta max}$ and core y location.

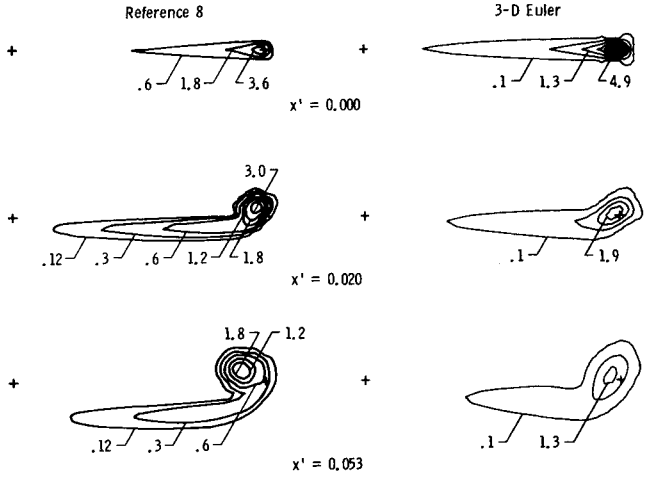

Fig. 8 Rectangular wing, comparison of streamwise vorticity contour plots with Ref. 8.

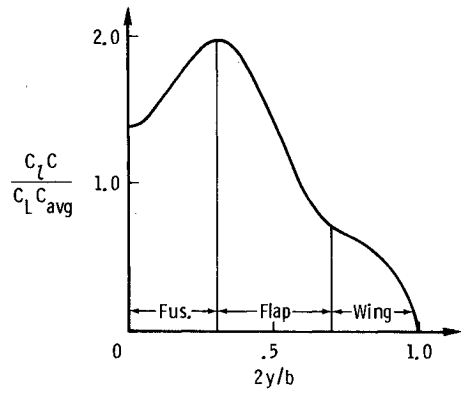

Fig. 9 Spanload distribution for the transport configuration.

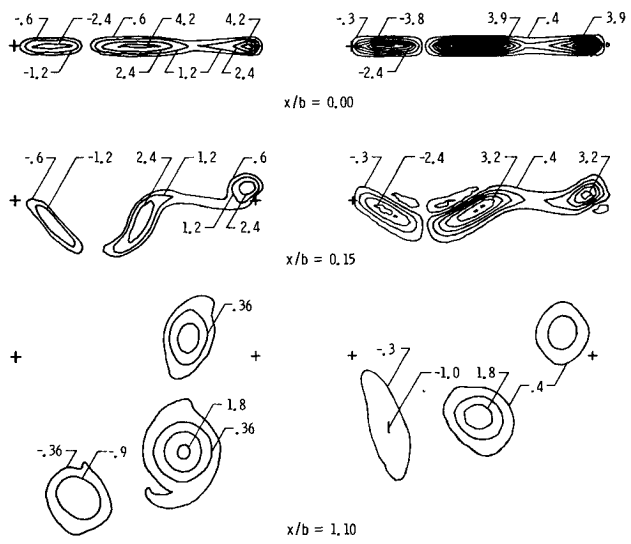

Fig. 10 Transport configuration, comparison of streamwise vorticity contour plots with Ref. 8.

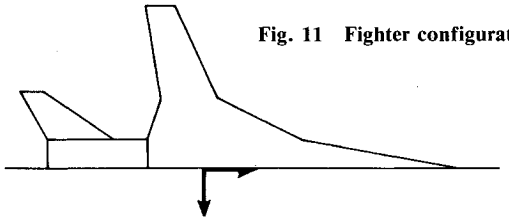

Fig. 11 Fighter configuration planform.

region is proportional to

$$b\frac{AR}{C_L}$$

where b is the span, AR is the aspect ratio, and C_L is the lift coefficient. Thus, when downstream locations among different results are compared, the scale distance x' must be the same

$$x' = \frac{x}{b}\frac{C_L}{AR}$$

Figure 8 compares results of this method with those of Ref. 8. Although the spanwise loading is essentially the same, the initial vorticity distribution used in Ref. 8 is obtained by placing a series of individual Lamb vortices along grids corresponding to the wing's trailing edge. Thus, direct quantitative comparison is not possible. However, as is seen in Fig. 8, good agreement between the two calculations is indicated. It should

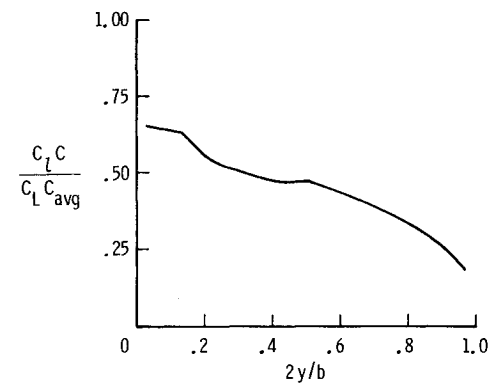

Fig. 12 Spanload distribution for the fighter configuration.

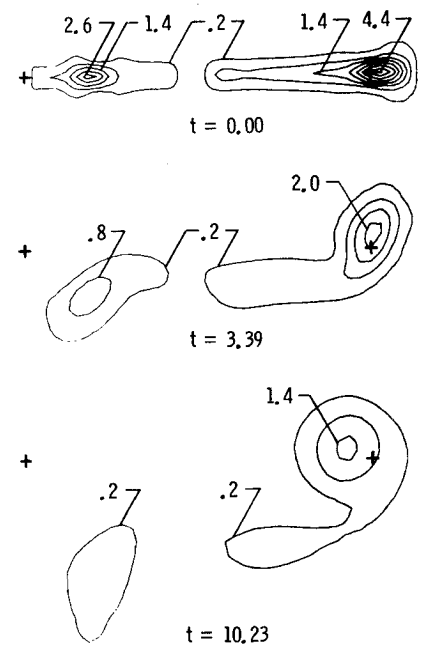

Fig. 13 Fighter configuration, streamwise vorticity contour plots.

be noted that these results also compare favorably with a second-order panel method.[13]

References 2, 8, and 13 also examined the wake resulting from a wing whose spanload distribution is similar to that found on large transport aircraft in landing or takeoff configuration. This spanload distribution (Fig. 9) was translated into a wing twist distribution for VLM input using a lifting line theory calculation. The resulting vorticity contours are compared (Fig. 10) with those of Ref. 8. As is seen from the figure, differences exist between the two calculations. These differences can be attributed to two main reasons. As mentioned above, Ref. 8 obtains the initial vorticity distribution by distributing a finite number of Lamb vortices. On the other hand, the initial vorticity distribution obtained here is from the vortex-lattice method. This is responsible for differences in the initial distributions indicated in Fig. 10. In addition, the boundary conditions used in Ref. 8 assume that vorticity decays exponentially with $(x^2+y^2)^{1/2}$, while the boundary conditions employed here are based on the method of characteristics. Thus, even if viscosity does not play a role in the roll-up region, these differences in initial and boundary conditions are significant enough to be responsible for the differences indicated in Fig. 10.

The final configuration considered illustrates the ability of this method to handle complex geometries. A fighter configuration was selected and is shown in Fig. 11. This is configuration 113 discussed in Ref. 10. It consists of a wing-body-

tail combination with a tail incidence of -10. A C_L of 1.0 was chosen, and the corresponding spanwise loading is indicated in Fig. 12. The streamwise vorticity distribution at different cross-plane locations is shown in Fig. 13.

Concluding Remarks

An Euler equation approach for modeling the initial roll-up of aircraft wakes was developed and evaluated. Inflow and initial conditions for the Euler calculation were provided by a vortex-lattice method solution of the lifting body being examined. The approach examined both three-dimensional solutions and unsteady two-dimensional solutions of the inviscid equations. These solutions appear to be in good agreement with available experimental data and other computational results. However, the available near-wake experimental data are limited.

For the geometries examined and the distances involved, the unsteady two-dimensional analogy was found to produce the same results as the full three-dimensional calculation at a savings of two orders of magnitude in computation time.

A convergence acceleration scheme for the three-dimensional calculation was found to increase convergence rates for the low Mach number cases examined here.

Acknowledgments

The authors would like to acknowledge many helpful discussions with Drs. C. H. Liu and R. P. Weston and Messrs. Jim Chamberlain and George C. Greene. Their continued guidance and help contributed greatly to the success of this effort. This research was supported in part by NASA Cooperative Agreement NCCI-84.

References

[1]Donaldson, C. duP. and Bilanin, A. J., "Vortex Wakes of Conventional Aircraft," AGARD-AG-204, May 1975.

[2]Hoeijmakers, H. W. M., "Computational Vortex Flow Aerodynamics," AGARD-CP-342, 1983.

[3]Margason, R. J., Kjelgaard, S. O., Sellers, W. L. III, Morris, C. E. K. Jr., Walkey, K. B., and Shields, E. W., "Subsonic Panel Methods—A Comparison of Several Production Codes," AIAA Paper 85-0280, Jan. 1985.

[4]Whitfield, D. L. and Janus, J. M., "Three-Dimensional Unsteady Euler Equations Solution Using Flux Vector Splitting," AIAA Paper 84-1552, June 1984.

[5]Jameson, A., Schmidt, W., and Turkel, E., "Numerical Solutions of the Euler Equations by Finite Volume Methods Using Runge-Kutta Time Stepping Schemes," AIAA Paper 81-1259, June 1981.

[6]Turkel, E., "Acceleration to a Steady State for the Euler Equations," NASA CR 172398, June 1984.

[7]Steger, J. L. and Kutler, P., "Implicit Finite Difference Procedure for the Computation of Vortex Wakes," *AIAA Journal*, Vol. 15, April 1977, pp. 581-590.

[8]Weston, R. P. and Liu, C. H., "Approximate Boundary Condition Procedure for the Two-Dimensional Numerical Solution of Vortex Wakes," AIAA Paper 82-0951, June 1982.

[9]Chigier, N. A. and Corsiglia, V. R., "Wind-Tunnel Studies of Wing Wake Turbulence," *Journal of Aircraft*, Vol. 9, Dec. 1972, pp. 820-823.

[10]Margason, R. J. and Lamar, J. E., "Vortex Lattice Fortran Program for Estimating Subsonic Aerodynamic Characteristics of Complex Planforms," NASA TN D-6142, Feb. 1971.

[11]Jameson, A. and Baker, T. J., "Multigrid Solution of the Euler Equations for Aircraft Configurations," AIAA Paper 84-0093, Jan. 1984.

[12]Weston, R. P., "Refinement of a Method for Determining Induced and Profile Drag from Detailed Wake Measurements," Ph.D. Dissertation, University of Florida, Gainesville, March 1981.

[13]Hoeijmakers, H. W. M. and Vaatstra, W., "A Higher Order Panel Method Applied to Vortex Sheet Roll-up," *AIAA Journal*, Vol. 21, April 1983, pp. 516-523.